Stress estimation in fifth wheel coupling system using finite element model validated by experimental modal test

Reza Ebrahimi[1*], Alireza Shafiei[2], Seyed Masoud Fatemi[2]
[1]*Assistant Professor, Mechanical Engineering, Faculty of Engineering, Yasouj University, Yasouj 75918-74831, Iran*

[2]*Research and Development Department, Espahan Koosha Company, Isfahan 81611-98371, Iran*

Abstract
In the heavy vehicle transport industry, the fifth wheel coupling system is used as important component for connecting the semi-trailer with the tractor. Misfunction, corrosion or fracture of the fifth wheel can affect the stability and consequently the safety of the heavy vehicles. During operation, the fifth wheel experiences different loading conditions. So, a reliable model which represents stresses due to acting forces on the fifth wheel coupling system plays a significant role. For this purpose, first, controlled vibration experiments are conducted on a JOST's fifth wheel coupling system and modal parameters of the system is obtained. Moreover, a finite element model (FEM) is constructed in ABAQUS software and successfully validated by the results of the experimental modal analysis (EMA). Then, the validated FEM is used to achieve the stress distribution in the system for accelerating and breaking conditions. Also, it is found that stresses in the JOST's fifth wheel coupling system remain below the mechanical strength limit of the material.

Keyword: Fifth wheel coupling system; Experimental modal analysis; Finite element modelling; Stress analysis.

1. Introduction
In order to provide a mechanical coupling between a towing tractor unit and a semi-trailer unit, the fifth wheel mechanism is employed in design of articulated heavy vehicles [1]. A typical fifth wheel is shown in Fig. 1. The stability and safety of articulated vehicles are directly dependent on the structural health of the fifth wheel system. Therefore, the stress analysis of the fifth wheel represents an active area of research [2, 3].

Fig. 1. A typical fifth-wheel coupling.

*Corresponding author. Tel.: +98-743-100-5000; FAX: +98-743-100-9555.
Authors' Email addresses: rebrahimi@yu.ac.ir (Reza Ebrahimi), shafiei.alireza1383@gmail.com (Alireza Shafiei), masoudfatemi@gmail.com (Seyed Masoud Fatemi).

Reboh et al. [4] developed a finite element model (FEM) of the fifth wheel system. Based on the British Standard BS 7608, they compared the finite element analysis with those given in the fatigue S–N curves. They reported that failure due to the fatigue occurs at the welded joint. Liu and Sun [5] studied the fatigue performance of the fifth wheels coupling system. They detected the saddle body positions that the fatigue damage easily occurs at them.

The dynamics of the cab and durability of the components can be affected by mounting position of the fifth wheel system on a semi-trailer [6]. Wideberg and Dahlberg [7] indicated that mounting the fifth wheel on a too far rearward position leads to a negative effect on the stability of the tractor-semitrailer. Miralbes et al. [8] simulated the wheels, the fifth wheel, the torsion bars and the suspension of the tractor unit by different types of elements. Then the most adequate model for the real behavior of the suspension and low computational cost was suggested. Nigam [9] developed a fifth-wheel model to inspect its effect on the vehicle behavior. During everyday driving, the fifth-wheel coupling experiences different working conditions. The number of tests were conducted on the fifth-wheel coupling to capture the interactions under different conditions. The results showed that the maximum reduction in amplitude of articulation angle can be reached when running a dry contact between the trailer and the fifth-wheel. Zhanga et al. [10] performed a scanning electron microscope metallographic and fractography evaluation to identify failure cases of the fifth wheel coupling. Batista et al. [11] utilized innovative sensors in fifth wheel design to monitor the vehicle dynamics for identifying the trailer swing effect. Wen et al. [12] redesigned the structure of the 90# fifth wheel. In this case the shape of each component has to be optimized for minimum weight, without change in the stiffness and strength of the fifth wheel.

In most cases, in situ stress measurement is difficult or impossible in the early stage of practical design [13-15]. Therefore, it is required to validate FEM by using the modal analysis techniques. In the last few years, several studies have been made on the experimental modal analysis (EMA). The EMA procedure is performed according to both force and response measurement data [16, 17]. On the other hand, operational modal analysis (OMA) techniques, such as stochastic subspace identification (SSI) and frequency domain decomposition (FDD), estimate the modal parameters directly from signal processing calculations and consider only output dynamic responses [18, 19].

It can be noted from the literatures that there is no published research considering structural and mechanical aspects of the fifth wheel coupling system with application of experimental modal analysis. Accordingly, in the present study, the FEM of a fifth wheel system is created in ABAQUS software and experimental modal analysis of the system is performed. The experimental modal test results are then employed for the validation of the constructed FEM. Finally, the stress distribution in the fifth wheel coupling system is estimated in using validated FEM.

2. Modal parameter extraction

The possibility of obtaining a modal model of the fifth wheel system will be briefly described in the following sections.

2.1. Theoretical aspects

For an undamped multi-degree of freedom system, with N degrees of freedom, the motion equations are typically expressed in the following condensed matrix notation:

$$[M]\{\ddot{x}(t)\}+[K]\{x(t)\}=\{f(t)\} \tag{1}$$

where $[K]$ is $N \times N$ stiffness matrix, $[M]$ represents $N \times N$ mass matrix, and $\{f(t)\}$ and $\{x(t)\}$ denote $N \times 1$ vectors of time-varying forces and displacements, respectively. Turning now to a response analysis, we suppose that the harmonic vector force $\{f(t)\}$ has a set of forcing functions with a common excitation frequency ω and individual magnitudes $\{F\}$. Then

$$\{f(t)\} = \{F\} e^{i\omega t} \tag{2}$$

So, the steady-state solution of Eq. (1) is given by

$$\{x(t)\} = \{X\} e^{i\omega t} \tag{3}$$

where $\{F\}$ and $\{X\}$ are $N \times 1$ vectors of time-independent complex amplitudes. The equation of motion then becomes

$$\left([K] - \omega^2 [M]\right)\{X\} e^{i\omega t} = \{F\} e^{i\omega t} \tag{4}$$

or rearranging to solve for the unknown responses,

$$\{X\} = \left([K] - \omega^2 [M]\right)^{-1} \{F\} \tag{5}$$

which may be written

$$\{X\} = [\alpha(\omega)]\{F\} \tag{6}$$

where $[\alpha(\omega)]$ is the $N \times N$ frequency response function (FRF) matrix for the system. The general component in the FRF or receptance matrix, $\alpha_{jk}(\omega)$, is given as follows:

$$\alpha_{jk}(\omega) = \left(\frac{X_j}{F_k}\right); \quad F_m = 0; \quad m = 1, N; \neq k \tag{7}$$

By considering Eq. (5), component values of the receptance matrix $[\alpha(\omega)]$ can be determined at different excitation frequencies. However, for this purpose, system matrix should be inverted at each frequency. Some disadvantages are linked to this mathematical operation, namely:

- The matrix inversion process at each frequency is costly for large-order systems (large N).
- This leads to extra operation, when only some of the individual FRF components are needed.

So, another form of the FRF is required which makes use of the modal properties (mode shapes and natural frequencies) for the system instead of the spatial properties (stiffness and mass matrices). Returning to Eq. (5) we can write

$$\left([K] - \omega^2 [M]\right) = [\alpha(\omega)]^{-1} \tag{8}$$

Premultiply both sides by $[\Phi]^T$ and postmultiply both sides by $[\Phi]$ to obtain to obtain

$$[\Phi]^T \left([K] - \omega^2 [M]\right)[\Phi] = [\Phi]^T [\alpha(\omega)]^{-1} [\Phi] \tag{9}$$

where $[\Phi]$ is the $N \times N$ mass-normalized mode shape matrix. So, the orthogonality properties of the mode shapes lead to

$$\left[\omega_r^2 - \omega^2\right] = [\Phi]^T [\alpha(\omega)]^{-1} [\Phi] \tag{10}$$

or

$$[\alpha(\omega)] = [\Phi]\left[\omega_r^2 - \omega^2\right]^{-1} [\Phi]^T \tag{11}$$

where ω_r is the r^{th} natural frequency, and $[\omega_r^2 - \omega^2]$ is a diagonal matrix. From Eq. (11), it has been argued that the receptance matrix $[\alpha(\omega)]$ is symmetric and this is recognized as the principle of reciprocity in structural engineering. The implication of this principle in the EMA leads to

$$\alpha_{jk} = \left(\frac{X_j}{F_k}\right) = \alpha_{kj} = \left(\frac{X_k}{F_j}\right) \tag{12}$$

Eq. (11) makes it possible to calculate any individual FRF expression, $\alpha_{jk}(\omega)$, using the following formula (noting that the resulting equation is obtained by multiplying the j^{th} row of $[\Phi]$ by the diagonal frequency matrix by the k^{th} column of $[\Phi]^T$):

$$\alpha_{jk}(\omega) = \sum_{r=1}^{N} \frac{(\varphi_{jr})(\varphi_{kr})}{\omega_r^2 - \omega^2} \tag{13}$$

This is a fundamental expression in the EMA [16]. According to Eq. (13), Bode plot of FRF has peaks corresponding to natural frequencies of the test object.

2.2. Vibration test

The test was conducted on a JOST's fifth wheel coupling system as shown in Fig. 2. The fifth wheel coupling system was vertically hung to simulate completely free boundary conditions. The fifth wheel coupling system was excited by an impact hammer with a force transducer (Global Test AU02). The dynamic responses were measured by four accelerometers (Global Test AP 2037-100) fixed at the corner of the test structure. An analyzer (SIRIUS) was utilized to record the force/acceleration signals and compute the frequency response functions (FRFs) between the measured accelerations and impact force. DewesoftX, a software for general purpose of data acquisition, was used to extract natural frequencies from the FRFs.

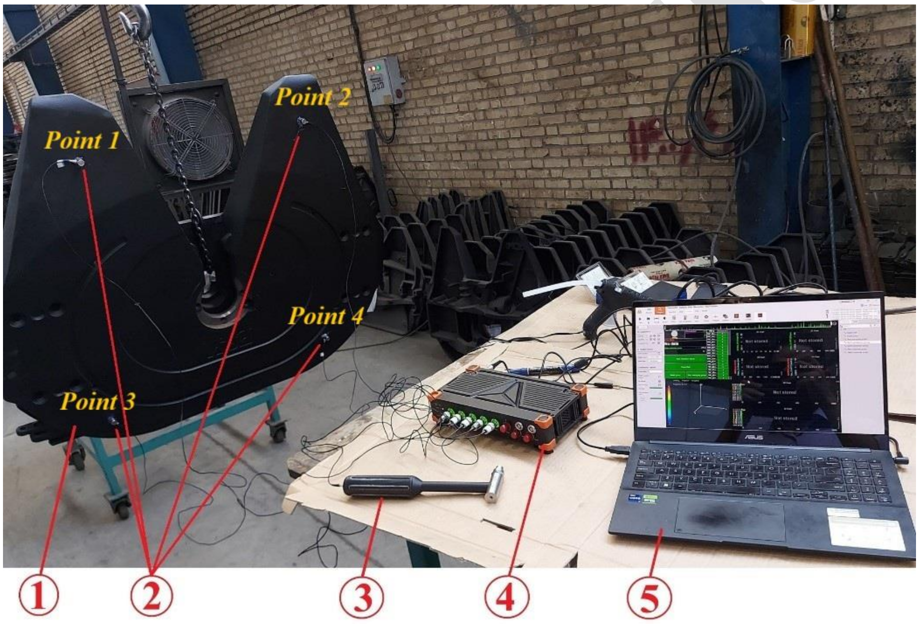

Fig. 2. Experimental setup of the fifth wheel coupling system: (1) JOST's fifth wheel coupling system (2) accelerometers (3) hammer with force transducer (4) analyzer (5) laptop computer with DewesoftX software.

Fig. 3 shows the some of the frequency response functions of the fifth wheel coupling system.

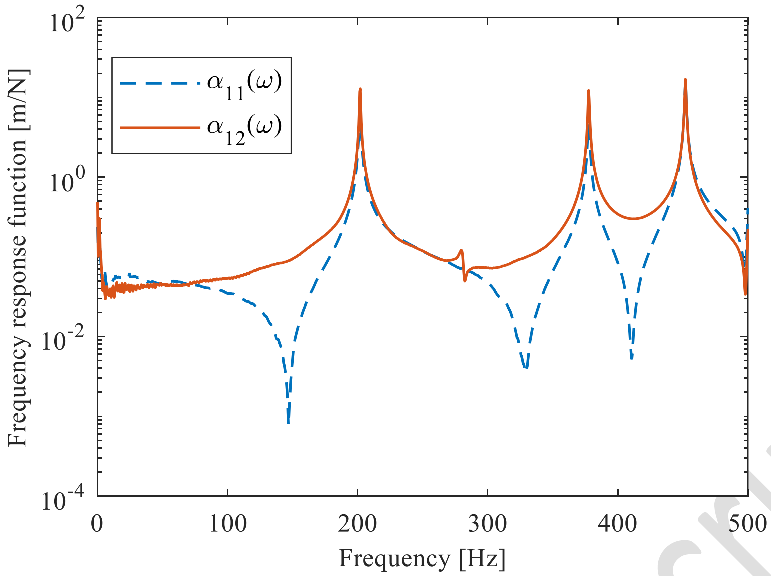

Fig. 3. Some of FRFs measured on the JOST's fifth wheel coupling system by experimental modal analysis.

3. Finite element model construction

Three-dimensional FEM of the JOST's fifth wheel coupling system has been constructed in the ABAQUS environment. The main plate, wearing ring, locking jaw, locking bar, king pin and bolts are modeled (Fig. 4). Then, these parts are assembled by employing the geometrical constraints, such as the face to face and coaxial constraints. After this, the properties of ductile iron (Young's modulus=*170* GPa, mass density=*7100* kg/m^3 and Poisson's ratio=*0.28*) are defined for the model. All parts are made from ductile iron according to the specifications presented in EN-GJS-400-18-LT. Free boundary conditions are considered for the frequency analysis. Fixed boundary conditions (at surfaces that contact with the base) are assigned to the model for the stress analysis. The tetrahedron elements is utilized to automatically mesh the model of the JOST's fifth wheel coupling system. The tie-surface constraint is also applied for the interactions of surfaces with various meshing.

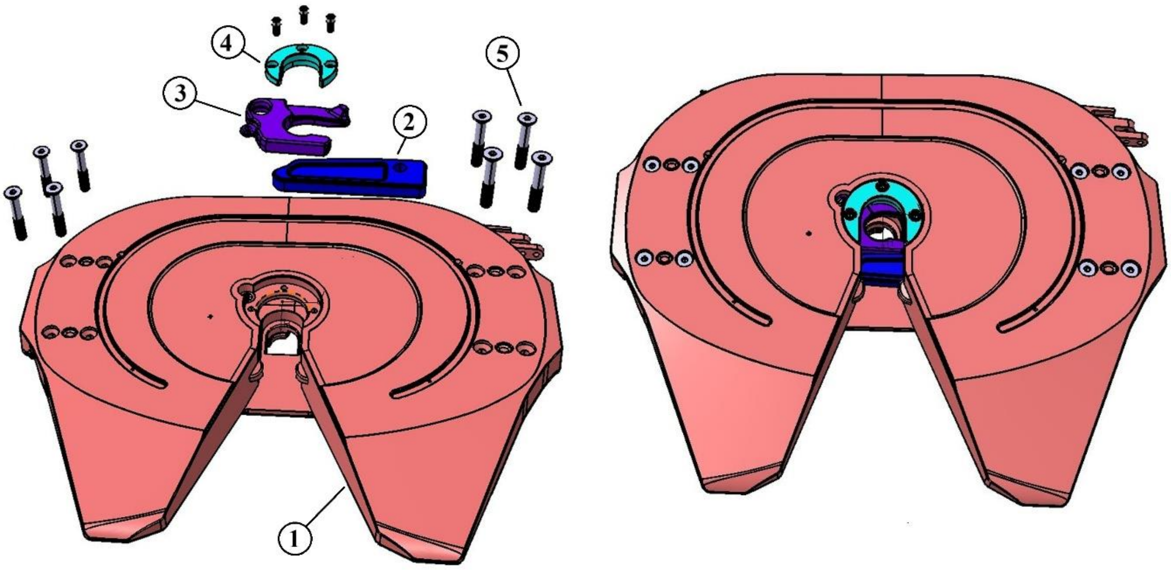

Fig. 4. Assembly model of the JOST's fifth wheel coupling system: (1) main plate (2) locking bar (3) locking jaw (4) wearing ring (5) bolts.

3.1. Frequency analysis

Selecting the geometrical and material properties which are required as the input values for the FEM simulation, may be rather questionable unless a validation procedure is used. So, a frequency analysis is carried out to calculate the natural frequencies and flexible mode shapes of the JOST's fifth wheel system. Then, the FEM is validated by comparing the simulated natural frequencies with those measured from the EMA. The simulation results obtained from the validated FEM can precisely descript mechanical behavior of the structure [20]. From Table 1, it can be observed that the simulation results (numerical natural frequencies) described the experimental results (measured natural frequencies) reasonably well and the maximum error on natural frequencies is about *1.2*%. It should be mentioned that, because of the free boundary conditions, the first six modes of the structure are typically "rigid body" modes. In the simulation, these six modes all occur at zero frequency. Up to six rigid body modes, flexible mode shapes can be found.

Table 1 Numerical and measured natural frequencies.

Flexible mode	Frequency [Hz]		Error [%]
	FEM	EMA	
1	*204.6*	*202.0*	*1.2*
2	*283.9*	*280.8*	*1.0*
3	*380.3*	*377.6*	*0.7*
4	*454.6*	*452.0*	*0.6*

Fig. 5 exhibits the first four flexible mode shapes of the JOST's fifth wheel coupling system for the natural frequencies calculated by using finite element model.

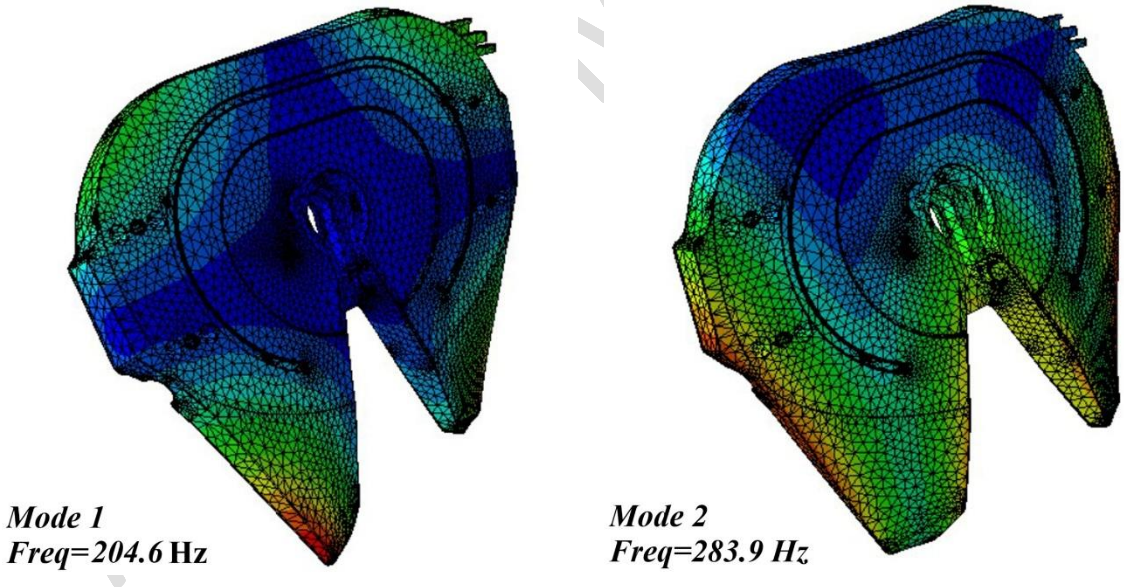

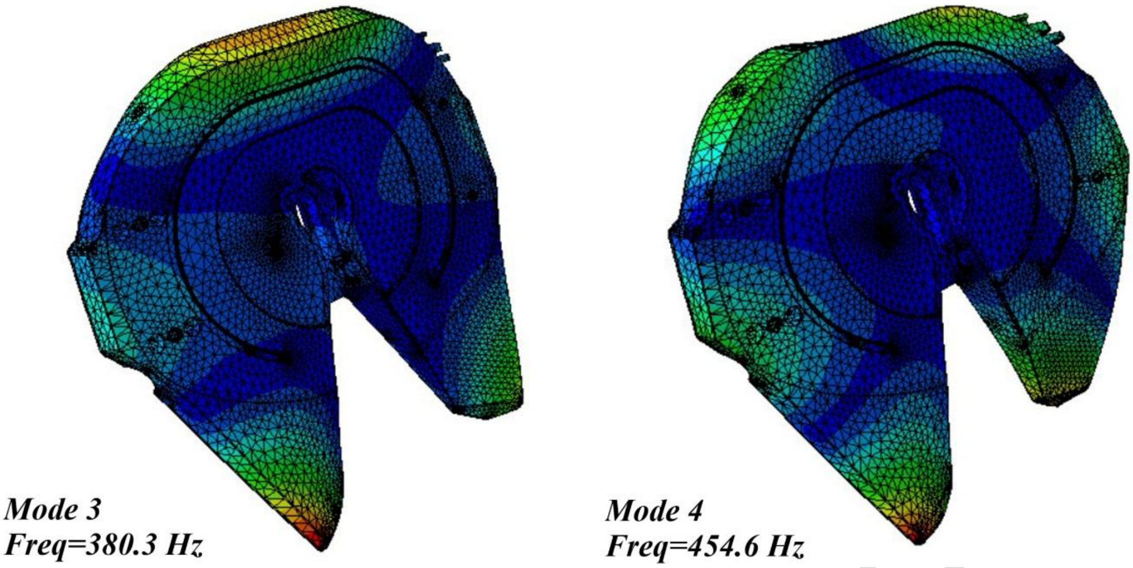

Fig. 5. The first four flexible mode shapes of the JOST's fifth wheel coupling system calculated by finite element model.

3.2. Stress analysis

After the verification process, the static analysis is executed to obtain the stress distribution of the fifth wheel coupling under external load. The fifth wheel coupling system is subjected to a variety of loading, because the heavy vehicles operate in different working conditions. The international standard ISO 8716 suggests the following load case for this type of connection:

$$F_h = g\frac{0.6m_1m_2}{m_1+m_2-m_3} \tag{14}$$

where F_h is the horizontal force applied to the kingpin, g is acceleration of gravity, m_1 is permissible total mass of the tractor unit, m_2 is permissible mass of the complete vehicle train which is pulled by the kingpin and m_3 is vertical mass exerted at the kingpin. The numerical values of these parameters are provided in Table 2. So, in ABAQUS software, the load equal to $F_h=0.0836$ meganewton is applied to the kingpin. Fig. 6 shows the fixed boundary conditions and the exerted force directions when the system is in accelerating and breaking conditions.

Table 2 Values of the loads applied to the fifth wheel coupling system.

Parameter	Value [ton]
m_1	*17*
m_2	*33*
m_3	*10.5*

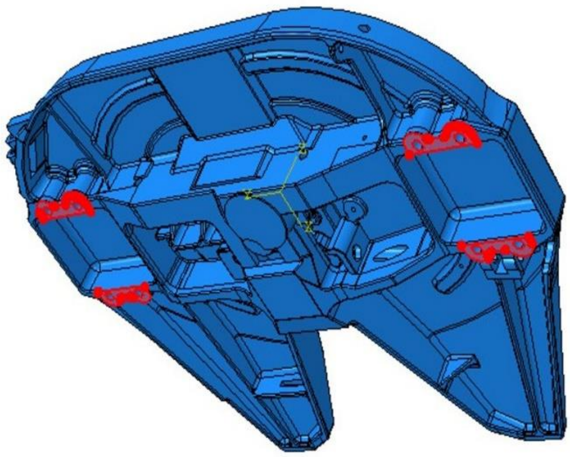

(a)

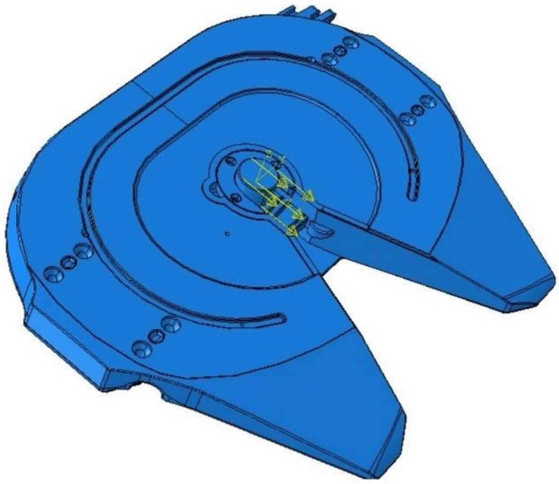

(b)

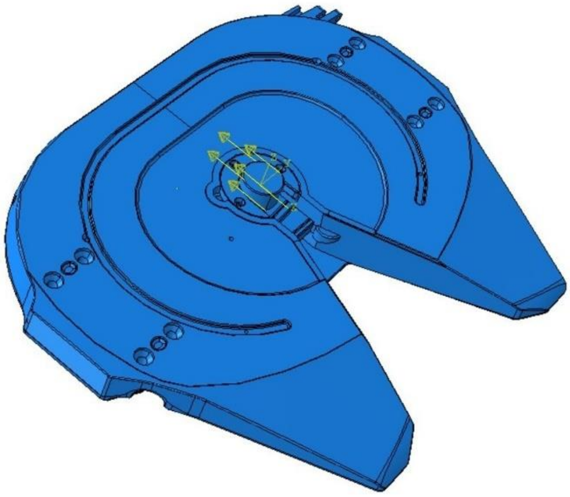

(c)

Fig. 6. Schematic of (a) fixed boundary conditions (b) force direction for accelerating conditions (c) force direction for breaking conditions.

When the articulated heavy vehicle is in acceleration condition, the maximum stress of *77.46* MPa is observed. By considering the breaking conditions, the maximum stress of *79.98* MPa occurs at the system (Fig. 7). The stress evaluation of the JOST's fifth wheel system reveals that the maximum stress does not exceed the mechanical strength limit of the material (σ_y=*350* MPa). Moreover, it can be concluded that the maximum Mises stress in the fifth wheel coupling under accelerating conditions is lower than the maximum Mises stress under breaking conditions.

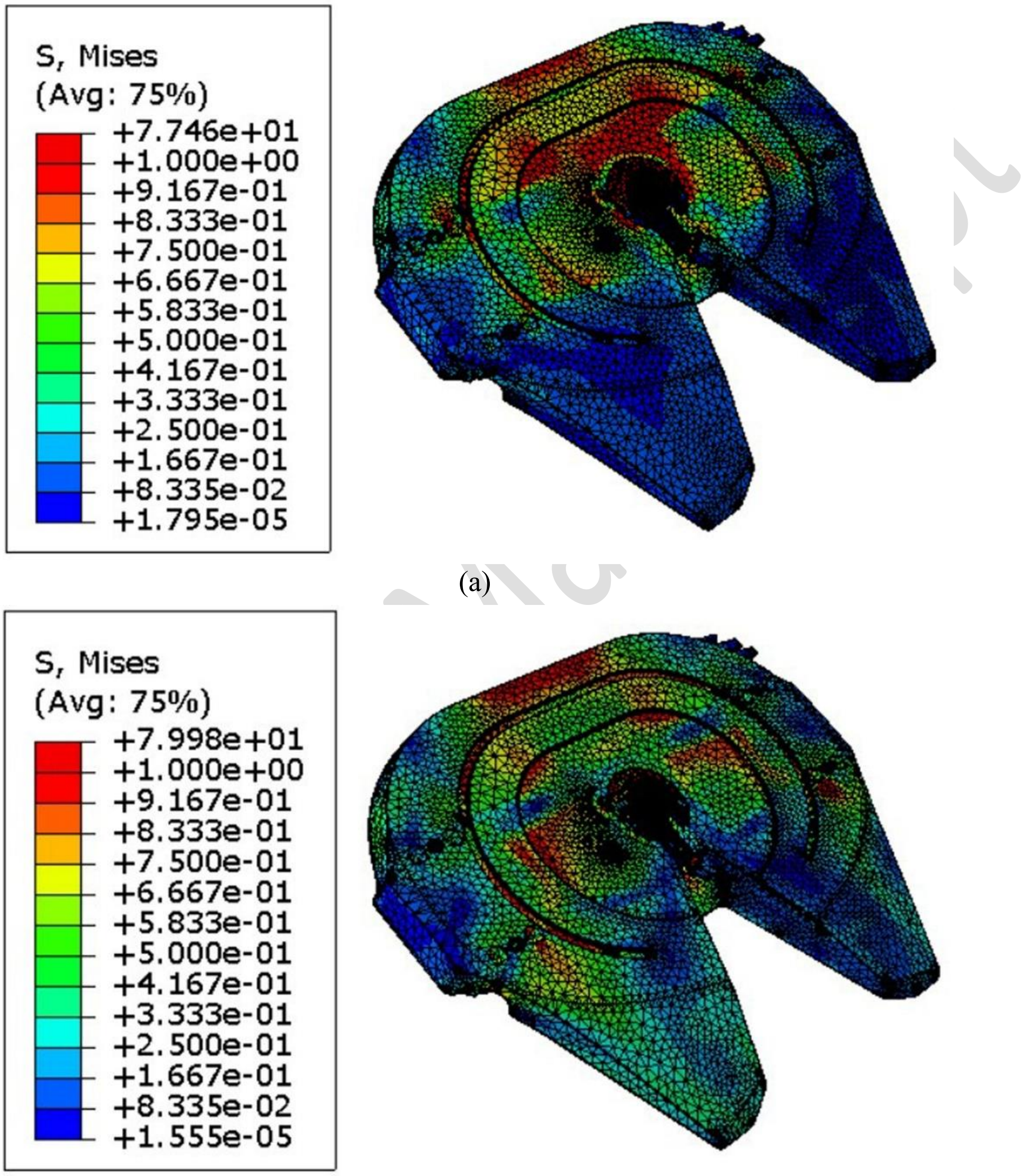

(b)

Fig. 7. Stress distribution of the JOST's fifth wheel coupling system: (a) accelerating conditions (b) breaking conditions.

4. Conclusions

This research represents the identification process of the vibration characteristics (natural frequencies) of the JOST's fifth wheel coupling system, on the basis of the experimental modal analysis (EMA). The results of EMA are used as a validation tool for the constructed finite element model (FEM). Then, the validated FEM is utilized for investigating the stress distribution and recognizing the high stress zones on this important structure. The stress evaluation of the JOST's fifth wheel system shows that, when the system is subjected to typical loading cases (accelerating and breaking conditions), the maximum stress remain below the mechanical strength limit of the material. Also, it is concluded that the maximum Mises stress in the fifth wheel coupling under accelerating conditions is lower than the maximum Mises stress under breaking conditions. At the end, the methodology presented in this paper can be generalized for further stress analysis in other machineries and structures.

References:

[1] P.J.L. Feanandes, Examination of a failed fifth wheel coupling, Engineering Failure Analysis, 5 (1998) 29–33.

[2] S. Bhat, S. Sheepri, Influence of fifth wheel position on cab durability and dynamics in tractor-semitrailer vehicle, SAE International Journal of Commercial Vehicles, 15 (2021) 189–199.

[3] A. Jogi, S. Chandramohan, Zero-speed off-tracking analysis of tractor-semitrailer with split fifth wheel coupling for 90° and 180° turning manoeuvres, In Advances in Mechanical Engineering, Proceedings of ICRIDME 2018, Singapore (2020) 1567–1578.

[4] Y. Reboh, S. Griza, A. Reguly, T.R. Strohaecker, Failure analysis of fifth wheel coupling system, Engineering Failure Analysis, 15 (2008) 332–338.

[5] Y. Liu, L. Sun, Fatigue life analysis of the fifth wheel saddle body, In Proceedings of the 2010 International Conference on Computer, Mechatronics, Control and Electronic Engineering (CMCE 2010), Changchun, China, (2020) 228–231.

[6] X. Liu, W. Chen, J. Zhao, T. Chang, X. Xu, The effect of fifth wheel location on handling stability of articulated vehicles, In Proceedings of the 2016 Annual Conference of the Chinese Society of Automotive Engineering, Shanghai, China, (2016) 951–956.

[7] J. Wideberg, E. Dahlberg, Effect of the fifth-wheel placement on the stability of articulated vehicles, International Journal of Heavy Vehicle Systems, 20 (2013) 144-156.

[8] R. Miralbes, J. Abad, D. Valladares, Simulation of suspensions, torsion bars, and fifth wheel for semitrailers using finite elements, Advances in Mechanical Engineering, 5 (2013) 548760.

[9] R. Nigam, Characteristics of fifth wheel and its influence on handling and maneuvering of articulated heavy vehicles, Master thesis, Chalmers University of Technology, 2018.

[10] Q. Zhang, S. Wei, Y. Chen, Failure analysis of the fifth wheel couplings utilized in heavy semitrailer tractors, Engineering Failure Analysis, 109 (2020) 104352

[11] I.A.A. Batista, N. Tomio, J.C.H. Gutierrez, Applicability study of fifth wheel sensors for monitoring the vehicle dynamics in articulated trucks, Brazilian Society of Automotive Engineering, (2021).

[12] W.E.N. Yanke, J.I. Hongchao, C.A.I. Zhongman, C.U.I. Guolong, Lightweight finite element analysis and experimental study of 90# fifth wheel, Mechanics, 30 (2024) 83-90.

[13] Y.S. Chen, C.S. Wang, Y.J. Yang, Combining vibration test with finite element analysis for the fatigue life estimation of PBGA components, Microelectronics reliability, 48 (2008) 638–644.

[14] F. Magalhaes, E. Caetano, A. Cunha, Operational modal analysis and finite element model correlation of the Braga Stadium suspended roof, Engineering Structures, 30 (2008) 1688-1698.

[15] R Ebrahimi, H.R. Mirdamadi, S. Ziaei-Rad, Operational modal analysis and fatigue life estimation of a chisel plow arm under soil-induced random excitations, Measurement, 116 (2018) 451-457.

[16] D. Ewins, Modal Testing: Theory and Practice, Research Studies Press, Herbfordshire, 1986.

[17] W. Heylen, S. Lammens, P. Sas, Modal Analysis Theory and Testing, Department of Mechanical Engineering, Katholieke Universiteit Leuven, 1995.
[18] R. Brincker, L. Zhang, P. Andersen, Modal identification of output-only systems using frequency domain decomposition, Smart Materials and Structures, 10 (2001) 441-445.
[19] Q. Wei, L. Shen, B. Kövesdi, L. Dunai, M. Cao, A lightweight stochastic subspace identification-based modal parameters identification method of time-varying structural systems, Journal of Sound and Vibration, 570 (2024) 118092.
[20] S. Rahmatalla, K. Hudson, Y. Liu, H.C. Eun, Finite element modal analysis and vibration waveforms in health inspection of old bridges, Finite Elements in Analysis and Design, 78 (2014) 40–46.

Figure Captions:

Fig. 1. A typical fifth-wheel coupling.

Fig. 2. Experimental setup of the fifth wheel coupling system: (1) JOST's fifth wheel coupling system (2) accelerometers (3) hammer with force transducer (4) analyzer (5) laptop computer with DewesoftX software.

Fig. 3. Some of FRFs measured on the JOST's fifth wheel coupling system by experimental modal analysis.

Fig. 4. Assembly model of the JOST's fifth wheel coupling system: (1) main plate (2) locking bar (3) locking jaw (4) wearing ring (5) bolts.

Fig. 5. The first four flexible mode shapes of the JOST's fifth wheel coupling system calculated by finite element model.

Fig. 6. Schematic of (a) fixed boundary conditions (b) force direction for accelerating conditions (c) force direction for breaking conditions.

Fig. 7. Stress distribution of the JOST's fifth wheel coupling system: (a) accelerating conditions (b) breaking conditions.

Table Caption:

Table 1 Numerical and measured natural frequencies.

Table 2 Values of the loads applied to the fifth wheel coupling system.